Nanoscale

Ultrabright fluorescent silica nanoparticles for in vivo targeting xenografted human tumors and cancer cells in zebrafish

Journal:	*Nanoscale*
Manuscript ID	NR-ART-07-2019-006371.R1
Article Type:	Paper
Date Submitted by the Author:	05-Oct-2019
Complete List of Authors:	Peerzade, Saquib; Tufts University Qin, Xiaodan; Boston University Laroche, Fabrice; Boston University Palantavida, Shajesh; Tufts University Dokukin, Maxim; Tufts University Feng, Hui ; Boston University Sokolov, Igor; Tufts University, ;

ARTICLE Nanoscale

Ultrabright fluorescent silica nanoparticles for in vivo targeting xenografted human tumors and cancer cells in zebrafish†

Received 00th January 20xx,
Accepted 00th January 20xx

DOI: 10.1039/x0xx00000x

Saquib Ahmed M. A. Peerzade[a], Xiaodan Qi[b#], Fabrice J.F. Laroche[b#], Shajesh Palantavida[c, ††], Maxim Dokukin[c, †††], Hui Feng[b*], Igor Sokolov[a,c,d*]

New ultrabright fluorescent silica nanoparticles capable of fast targeting of epithelial tumors in vivo are presented. The synthesized folate-functionalized ultrabright particles of 30-40 nm are 230 times brighter than quantum dots (QD450) and 50% brighter than polymer dots of similar spectra (excitation 365 nm / emission 486 nm). To decrease non-specific targeting, particles are coated with polyethylene glycol (PEG). We demonstrate the targeting of xenographic human cervical epithelial tumors (HeLa cells) in-vivo using zebrafish as a model system. The particles show targeting tumors (and probably even individual HeLa cells) as small as 10-20 microns within 20-30 minutes after blood injection. To demonstrate the advantages of ultrabrightness, we repeated the experiments with similar but 200x less bright particles. Compared to those, ultrabright particles showed ~3x faster tumor detection and ~2x higher relative fluorescent contrast of tumors/cancer cells.

1. Introduction

Fluorescent nanoparticles are of large interest for cancer detection.[1] Fluorescent particles of high brightness are of particular interest for biology and medicine because of easy detection, less phototoxicity produced by excitation light during observation (fewer particles required).[2-5] The use of less concentration of ultrabright nanoparticles further reduces the potential toxicity of nanoparticles them self. High brightness also allows for faster detection of targeted objects, decreasing phototoxicity [6, 7] because a smaller number of targeting fluorescent particles is needed to develop detectable signal above the background threshold. Since the number of such particles is proportional to time, the smaller number of particles needed for the detection, and thus, the faster the target can be detected. Finally, when using for tissue, the fluorescent signal could be detected from the deeper regions of the tissue due to the higher brightness.

Mesoporous (sometimes called nanoporous) silica nanoparticles are attractive for biomedical applications due to their ability to carry high payloads.[8, 9] Various dyes [10-12] and drugs [13] can be incorporated inside nanoscale pores of these particles. Ultrabright fluorescent mesoporous silica (UFMS) nanoparticles (brighter than quantum dots of similar size and spectra) have been created in this way, including ultrabright NIR fluorescent particles that are useful for nontransparent tissue. [8, 14, 15] It was demonstrated that dye could be encapsulated at a very high concentration in the mesoporous silica matrix without quenching their fluorescent efficiency. For example, 50 mM of rhodamine 6G dye can be loaded with virtually no change in the dye quantum yield, which is almost three orders of magnitude higher than the quenching concentration of free dye in water.[10, 11, 16] Because of physical encapsulation of dyes inside silica nanochannels, a particular care should be taken with respect to the dye leakage, which was initially a substantial problem.[9] This problem was addressed by using a small number of hydrophobic groups added to the silica matrix. Together with small geometry of nanoscale channels (3-5nm in diameter), it allowed creating a substantially hydrophobic environment inside the channels to prevent water from moving in.[8] Later, it was demonstrated that this approach is independent of the type of hydrophobic groups by using different organotriethoxysilanes. [11] In the same reference, the long-term stability of the dye inside the particles (up to 120 days) as well as colloidal particle stability was demonstrated. Ultrabrightness is achieved due to a special nanoscale environment of the dye molecules created by the silica matrix and surfactant tails.[10] Each dye molecule is caged inside silica nanochannels, having an almost free rotation but rather a slow diffusion along the channels. Such confinement prevents collisional fluorescent quenching, and hence, maintaining high quantum yield. The close proximity of the encapsulated dye molecules allows combining different dyes within a single UFMS particle to create different complex spectra, which can be excited with a single wavelength. [12]

Despite the advantages mentioned above, ultrabright silica particles could not be used for in vivo applications, which require coating of the particles with specific molecules as well as the stealth molecules to prevent non-specific targeting. Because ultrabrightness is maintained through a delicate balance between the Brownian motion of the dye and confinement of the nanoscale environment of the silica matrix, it is quite easy to break this balance during an attempt to functionalize such particles with a tagging molecule. As an example, just standard silane chemistry dramatically decreases

[a] Department of Biomedical Engineering, Tufts University, Medford, MA 02155, USA. Email: igor.sokolov@tufts.edu
[b] Departments of Pharmacology and Medicine, The Cancer Research Center, Section of Hematology and Medical Oncology, Boston University School of Medicine, Boston, MA, USA. Email: huifeng@bu.edu
[c] Department of Mechanical Engineering, Tufts University, Medford, MA 02155, USA.
[d] Department of Physics, Tufts University, Medford, MA 02155, USA.
††Present address: Center for Nano and Material Sciences, Jain University, Jakkasandra, Kanakapura, Karnataka 562112 India.
††† National Research Nuclear University MEPhI, Moscow, 115409 Russia
# Equal contribution

†Electronic Supplementary Information (ESI) available: [details of any supplementary information available should be included here]. See DOI: 10.1039/x0xx00000x

the particle fluorescence. Previously, we have suggested two possible functionalization solutions which retained the particle ultrabrightness. Folate-functionalized ultrabright mesoporous silica nanoparticles were shown to be internalized by human cervical epithelial cells. [6] The sensitivity of 95-97% and specificity of 94-95% was demonstrated for the detection of cervical cancerous cells in-vitro. [6] However, those particles were not protected from nonspecific interactions, and therefore, were not suitable for in-vivo applications. In addition, the targeting molecules should be attached to a spacer to stand above the protecting coating. These are two major challenges addressed in the present work.

A popular way to prevent the nonspecific attraction of the particles to other objects/molecules besides the target is to coat particles with PEG molecules. [17] It is well developed on, for example, quantum dots. [18, 19] In the literature, mesoporous silica nanoparticles are PEGylated by first removing surfactant. [20] As was noted, this is not the option for ultrabright nanoparticles because it would destroy ultrabrightness.

In this work, we report on the development of ultrabright fluorescent silica nanoparticles for in-vivo applications, which are coated with PEG and functional molecules (folic acid) attached to PEG spacer. We demonstrate the use of such particles for the detection of human cervical cancer metastasis in zebrafish. Because of the optical transparency of zebrafish, we can work with fluorescent dyes of the visible spectrum. To avoid spectral overlap with the fluorescence of cervical cancer cells that are genetically engineered to express a red fluorescent protein (RFP) and to avoid auto-fluorescence of background, we developed ultrabright fluorescent silica nanoparticles in the blue part of the spectrum. We have synthesized folate-functionalized UFMS nanoparticles (30-40nm in size) which are ~230 times brighter than quantum dots of comparable spectrum (QD450 by ThermoFisher) and 50% brighter than polymer dots of similar (blue) spectra reported in the literature. [21] Using these particles, we have demonstrated specific tumor (or cancer cells) targeting in vivo in zebrafish model with sensitivity (accuracy of the detection) up to 94% (while specificity, the accuracy of not falsely targeting healthy tissue, is up to 87%). As small as 10-20 microns within the first 20-30 minutes of injection into the fish blood can be detected.

2. Results and Discussion

Particle characteristics

Previously reported procedure was modified for synthesizing mesoporous silica nanoparticles,[11, 22] see the Experimental section for detail. Stilbene 420 dye was encapsulated in mesoporous silica nanoparticles (SiSB particles). To decrease nonspecific interactions of particles with various surfaces and molecules in vitro, and in particular in vivo,[17] the particles were covered with polyethylene glycol (PEG) molecules. In principle, it can be done using three different ways: covalent coating with pre-synthesized PEG-silane which was added in the synthesizing bath of SiSB particles, physical coating with copolymer PF127, and a combination of these two approaches. Because physical coating does not change optical properties of the particles and only slightly increase their size (by the size of the coating), we investigate physical and optical properties of the particles coated with PEG covalently, SiSB-PEG.

Functionalization with folates was done in a similar manner, and consequently, three different PEGylated and folate functionalized particles were synthesized: using a covalently pre-synthesized folic acid-amine conjugates which were added in the synthesizing bath of the particles, by using physical coating with pre-synthesized PF127-folic acid (PFFA) conjugate, and a combination of these two approaches. Here we look at the following PEGylated and folate-functionalized ultrabright fluorescent silica nanoparticles: SiSB-PEGFA-PEG (particles synthesized as described above with PEG silane and Folic acid- acid-amine (AHAMTES)), SiSB-PFFA (particles coated with only PFFA), SiSB-PEGFA-PFFA (particles with folic acid AHAMTES, PEG-silane and PFFA).

Figure 1 shows the physical and optical characteristics of ultrabright SiSB particles. These characteristics are similar to all particles described in this work independently of functionalization. The excitation and emission matrixes of Stilbene 420 dye (aqueous solution in water at 0.1 μM concentration, for absorbance spectra of SB dye and SiSB particles, see supplementary information figure S1) and Stilbene 420 encapsulated mesoporous silica nanoparticles (SiSB particles; water dispersion of 0.1 nM) are shown in the Figures 1A and B. Stilbene 420 dye has a maximum peak around 430nm whereas SiSB particles show two peaks at 410 and 430 nm, which presumably indicates that there is an ionic interaction between the used surfactant cetyltrimethylammonium bromide (CTAB) and Stilbene 420 dye in agreement with previously reported in ref.[23]

The particles size was measured using dynamic light scattering (DLS), see Table 1 for detail. Figure 1C shows an AFM image of individual particles. The average size of the particles measured using AFM agrees with the DLS results (also see, figure S2, table S1 & S2). Figure 1D demonstrates the photostability of the synthesized particles. Normalized fluorescence intensity of free dye solution (empty circles) and particles (filled circles) of the same optical density are shown after irradiating with the white light of 450W xenon lamp for the duration of up to 90 seconds. Each value is the average of 10 measurements. One can see that particles show higher photostability compared to the dye itself. Using the exponential decay law (a*e(-b*t)+c), we can see that the rate constant b of the particles bleaching is 1.7x less compared to free dye (0.017 s-1 versus 0.029 s-1). This indirectly confirms that the dye is encapsulated inside the particles because encapsulation protects the dye molecules from excessive thermal degradation and oxidation. It should be noted that the absence of leakage of the encapsulated dye from such type of particles is in agreement with the previous reports. [8, 9, 11] This high photostability was observed for all other silica-encapsulated dyes described in this work.

Table 1 shows the major characteristics of the synthesized particles, which are measured using methods described in the

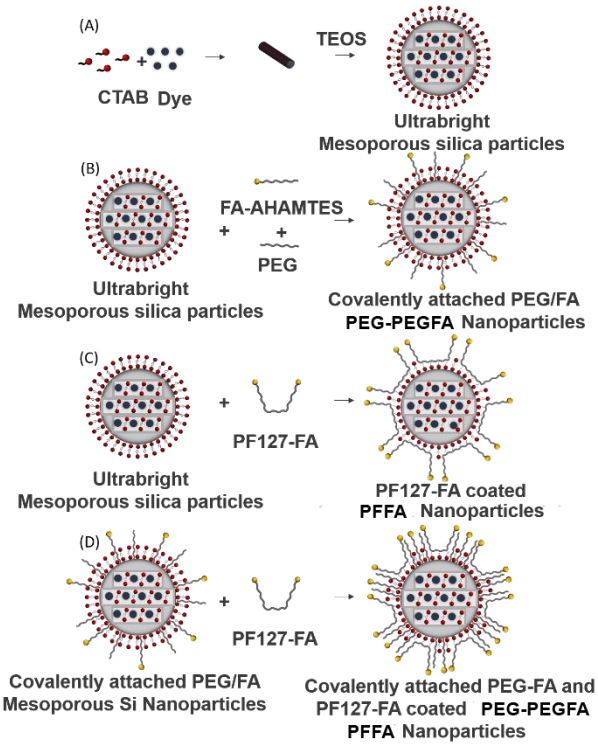

Scheme 1: Schematic illustration of the methods used to synthesize ultrabright mesoporous silica nanoparticles (A). Synthesis of ultrabright mesoporous silica nanoparticles with covalent attachment of folic acid and PEG (B). Coating ultrabright mesoporous silica particles with PF127-FA (C). Coating covalently attached PEG-FA mesoporous silica nanoparticles with PF127-FA (D).

Experimental section and Supplementary information. The particle size distribution is measured by means of dynamic light scattering (DLS). Note: Two sizes are shown, the most probable (number average) size and the Z-average size. Out of these two sizes, the most relevant to the actual particle size is the number average, which is the size of the most abundant particles. In the presence of large aggregates, the average size can be artificially large. The absence of a substantial difference between these two sizes is a good indication of monodispersity of the synthesized particles.

Scheme 1 shows several methods of functionalization and synthesis of mesoporous silica nanoparticles with PEG-PEGFA (Scheme 1B), PFFA (Scheme 1C) and the combination of PEG-PEGFA and PFFA (Scheme 1D). One can see that the number average size of SiSB increased from 33 ± 2 nm to 40 ± 1 nm upon coating with PFFA (Table 1). When covalently attaching (3-Aminopropyl) triethoxysilane-PEG (APTES-PEG) and N-(6-aminohexyl) aminomethyltriethoxysilane-FA (AHAMTES-FA) to SiSB nanoparticles to obtain SiSB-PEGFA, the particle size remained roughly constant with the number average of 34 ± 1 and 31 ± 2 nm, respectively. To increase the number of folate molecules per particles, SiSB-PEGFA particles were coated with PFFA. Upon addition of PFFA, the size of SiSB-PEGFA particles increased from 31 ± 2 nm to 38 ± 2 nm. The increase in size after coating PFFA on both SiSB and SiSB-PEGFA was ~ 7 nm. This increase can be attributed to the PFFA layer coating the particles. Thus, the thickness of PFFA coating on the particles may be estimated to be ~ 3.5 nm.

The zeta potential of particles is an indirect indicator of the particle surface modification. One can see from Table 1 that it is +42 mV for SiSB-PEGFA nanoparticles; it decreases to +33 mV upon grafting of PEG, which is in agreement with the presence of additional neutral PEG molecules. Coating SiSB and SiSB-PEGFA with PFFA decreases the zeta potential to +18 mV. Folate molecules, being negative in neutral pH, should result in a decrease of the zeta potential. Thus, the observed behaviour confirms indirectly the coating of the particles with folates.

Table 1: Properties of the synthesized particles: Number weighted, Z-average sizes, relative fluorescence brightness of ultrabright mesoporous silica nanoparticles in both MESF units (relative to one free dye molecule) and M^{-1} cm^{-1}, number of dye molecules per particle, quantum yield of the dye molecules after encapsulation (QY), poly-dispersity index (PDI), the zeta potential of nanoparticles, and the number of folate groups per particle.

Particle type	Number weighted average (nm)	Z-average (nm)	Relative Brightness MESF units	QY	Relative Brightness (M^{-1} cm^{-1})	Number of dye molecules per particle	Zeta potential (mV)	PDI	No. of FA per particle
SiSB	33 ± 2	53 ± 0.2	740 ± 40	0.79	(470 ± 10) x10^5	790 ± 20	+42 ± 4	0.14	N/A
SiSB-PEG	34 ± 1	64 ± 0.3	690 ± 20	0.57	(450 ± 10) x 10^5	990 ± 30	+40 ± 2	0.17	N/A
SiSB-PEGFA-PEG	31 ± 2	58 ± 0.4	360 ± 30	0.15	(230 ± 30) x 10^5	1910 ± 190	+33 ± 3	0.24	820 ± 80
SiSB-PFFA	40 ± 1	69 ± 0.6	350 ± 20	0.16	(230 ± 10) x 10^5	1770 ± 100	+17 ± 1	0.21	4100 ± 210
SiSB-PEGFA-PFFA	38 ± 2	67 ± 0.6	214 ± 17	0.1	(140 ± 7) x 10^5	1720 ± 150	+19 ± 1	0.21	4400 ± 420

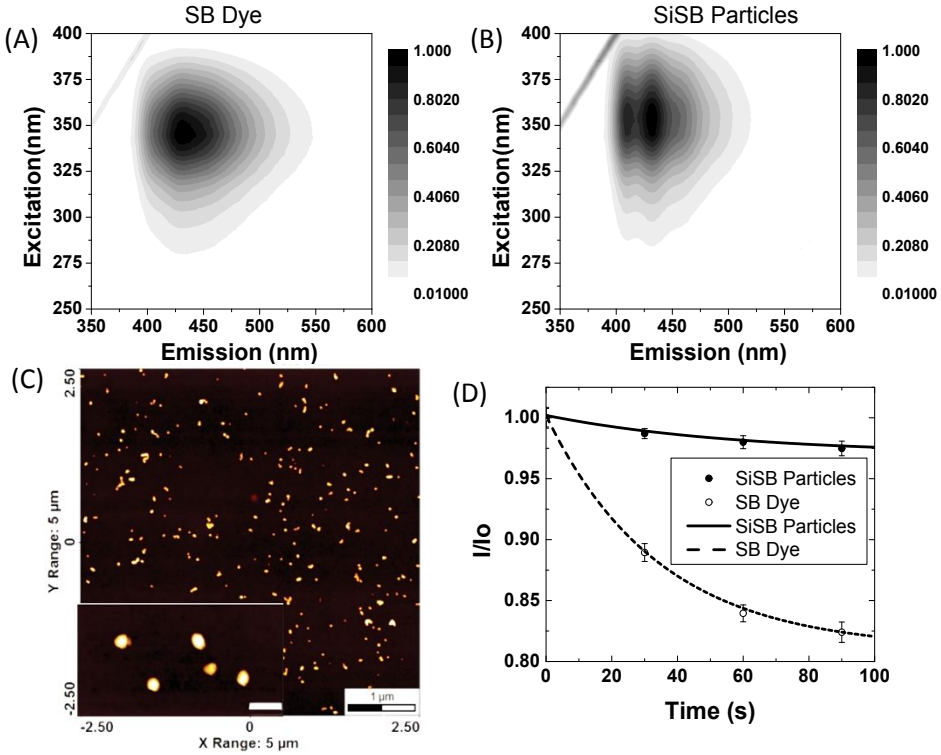

Figure 1. Characterization of ultrabright Stilbene 420 encapsulated mesoporous silica nanoparticles. (A) Excitation and emission matrix of stilbene 420 dye and (B) UFMS nanoparticles with encapsulated stilbene 420 (SiSB). (C) AFM of SiSB nanoparticles with inset showing zoomed image of nanoparticles (insert scale-bar is 100nm). (D) Fluorescent photostability of ultrabright silica particles (filled circles) relative to a water solution of Stilbene 420 dye (empty circles); the solid and dashed curve corresponds to the exponential fits of bleaching.

The number of folate molecules per particle on coated particles was determined by measuring folate optical absorbance in the particles (see the Supplementary information, Figure S4). As was shown in [5], this method is in good agreement with the results obtained with Raman spectroscopy. The number of folic acid molecules was 4800, 3950, 1340 for SiSB-PEGFA-PFFA, SiSB-PFFA, and SiSB-PEGFA particles, respectively. In the case of the use of amine-folic acid conjugate, some of the folates can be encapsulated inside the volume of the particles. Therefore, these density numbers should be treated as an upper limit for those particles.

Table 1 also shows the particle brightness to relative fluorescence of one free dye molecule in so-called MESF (Molecules of Equivalent Soluble Fluorochrome) units. The details of the measurements are presented in the Supplementary information, section 5 "Measurements for quantifying brightness and quantum yield of the particles". These units are broadly used in flow cytometry and in the characterization of particle brightness. [14, 24-28]

One can see that this brightness depends on the method used to functionalize particles. Brightness is the highest (~690) for covalently attached PEG (SiSB-PEG). (It corresponds to the dye concentration inside the particles 66 ± 1 mM.) After attaching folic acid covalently, the brightness decreased to 360. After coating PFFA on bare SiSB and SiSB-PEGFA nanoparticles, the brightness dropped to 350 and 214, respectively.

It should be noted that there is another well-known method of calculation of the fluorescent brightness. The brightness of the particles can be calculated as follows [29]

$$B = \varepsilon(\lambda)\phi \quad (1)$$

$$= \frac{Absorbance * \phi}{Concentration\ (M) * l(cm)},$$

$$B = \frac{IF}{Concentration\ (M) * l(cm)}, \quad (2)$$

where $\varepsilon(\lambda)$ is the extinction coefficient as a function of wavelength λ, ϕ is the quantum yield and IF is the integral fluorescence for a particular excitation wavelength.

We will show that these two definitions are equivalent. The ratio of brightness of particles is to dye calculated using the product of extinction coefficient and quantum yield (equation 1) is given by

$$\frac{B_{particles}}{B_{dye}} = \frac{IF_{Particles}/Concentration\ (M)_{particles} * l(cm)}{IF_{dye}/Concentration\ (M)_{dye} * l(cm)},$$

$$= \frac{IF_{Particles}/Concentration\ (M)_{particles} * Na}{IF_{dye}/Concentration\ (M)_{dye} * Na},$$

$$\frac{B_{particles}}{B_{dye}} = \frac{IF_{Particles/Number\ of\ particles}}{IF_{dye/Number\ of\ dye\ molecules}}, \quad (3)$$

$$= Relative\ Brightness.$$

Equation 3 shows that the ratio of brightness of particles to dye calculated using the product of extinction coefficient and quantum yield (equation 1) is equal to the relative brightness. The extinction coefficient of SB dye at 350 nm wavelength was 79100 ± 500 M^{-1} cm^{-1}. The quantum yield of the dye encapsulated particles was calculated (using Stilbene 420 dye as a reference, see supplementary information figure S5-8) through equation S1 (see the Supplementary information). The brightness of SiSB particles and SB dye calculated using equation 1 was (48 ± 1) x 10^6 and 64860 ± 440 M^{-1} cm^{-1}, respectively. The ratio of the brightness of SiSB particles (B) to that of SB dye calculated using equation 3 was 740 ± 40. Note that the particle diameter was estimated using the DLS technique. It may lead to a slight overestimation of the particle size due to the fact that hydrodynamic radios measured in DLS is larger than the size of actual silica core.

To verify ultrabrightness, we compare the brightness of the obtained particles with that of quantum dots of similar spectra, QD450. Brightness of these quantum dots is 1 x 10^5 M^{-1} cm^{-1} ,[30] while that of SiSB particles is (470 ± 10) x 10^6 M^{-1} cm^{-1} assuming 33 nm size. This shows that SiSB particles are 470 times brighter than QD450 particles. The brightness of UV polymer dots of size 67 nm reported in literature [21, 31] is 1.7 x 10^8 M^{-1} cm^{-1}. As was shown in [10], the particle brightness is proportional to its volume. Furthermore, the particle volume can be easily controlled towards the increase of the particle size.[10] If we compare the brightness of the polymer dots with our particles of 67 nm in size, SiSB particles are 2.5 times brighter than the brightest UV polymer dots. Similar calculations done for the folate functionalized particles show that the particles (SiSB-PEGFA-PEG) are ~230x brighter than QD450 quantum dots and 1.5x brighter than the brightest UV polymer dots (supplementary information, Sec. 5 for detail).

It is worth comparing the brightness of our UFMS particles with silica-based UV fluorescent 110 nm particles reported previously.[32] Those particles were claimed to have a brightness of 10^5 pyrene molecules per particle. The extinction coefficient of the fluorescent compound incorporated in those particles was 35000 cm^{-1} M^{-1} at 345nm, and the extinction coefficient after encapsulation dropped to 23300 cm^{-1} M^{-1}. Quantum yield of the fluorescent compound after encapsulation was 0.48. Scaling the brightness of the particles to the size of UFMS stilbene-encapsulated nanoparticles, one can see that our UFMS particles are 50% brighter than the particles of ref.[32] Compared to pyrene doped silica particles, the size of UFMS particles can be easily controlled.[10] Furthermore, the synthesis of UFMS nanoparticles does not require functionalization of dyes with silane groups, which is a required limitation for the other dye-doped particles (dye needs to be functionalized with silane groups for covalently attaching with silica core; [33] not all dyes can be attached with silane groups).

Verification of tagging ability of UFMS particles using human cervical epithelial cancer (HeLa) cells in vitro

To verify biological tagging activity of folate-functionalized particles, we use human cervical epithelial cancer (HeLa) cells in vitro. These cells have overexpressed folate receptors.[34] This is a transporter-type receptor. It means that the concentration of folate-functionalized particles inside such cells should increase with time. As a control, we used the same particles but without folate molecules. The particle suspensions were added to sub-confluent HeLa cells grown in a culture dish. The final concentration of particles in the dish was 0.1 mg/mL. The cells were incubated with the particle suspensions for 20, 50, and 90 minutes. After changing the media, cells were imaged with a fluorescent microscope (the light illumination and camera exposure were kept the same for all samples and incubation times during measurements of fluorescence intensity).

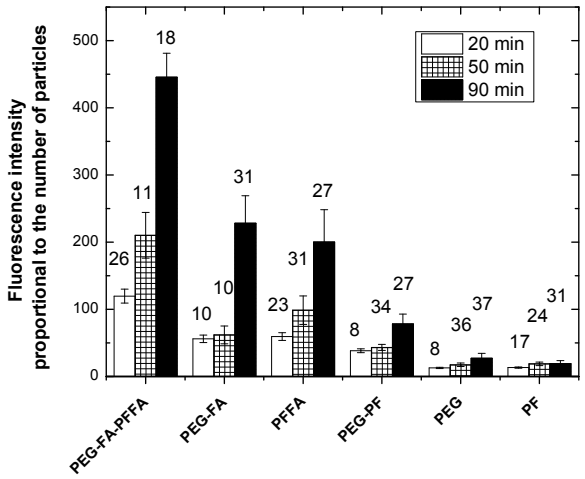

Figure 2. Fluorescence intensity (in arbitrary units), which is proportional to the number of UFMS particles accumulated in cells after 20, 50, and 90 minutes of incubation. (Raw fluorescence intensities per unit area were divided by a coefficient shown in Table S5 to compensate for various brightness of different particle types.) The number above each column bar represents a number of analysed cells. Error bars indicate the standard deviation between different tumours in Zebrafish. The results for folate functionalized particles (SiSB-PEGFA-PFFA, SiSB-PFFA, SiSB-PEGFA) and no-folate controls (SiSB-PEG-PF, SiSB-PEG, SiSB-PF respectively) nanoparticles are shown. The experiments were repeated 3 times, three independent wells of a multiwell seeded in parallel and treated in parallel, a picture of each was acquired.

Figure 2 summarizes results of the measurements of fluorescence intensity per unit area (calculated within the cell area), adjusted to the brightness of SiSB-PEG particles (Table S5). This way it is approximately proportional to the number of fluorescent particles accumulated in cells. Examples of fluorescent images of cells coated with folate- functionalized and control particles are shown in Figure S10.

One can see that all folate functionalized particles (SiSB-PEGFA-PFFA, SiSB-PEGFA-PEG and SiSB-PFFA) show both a larger number of internalized particles and significant increase of the number of internalized particles with time. The control particles similarly coated but without folates (SiSB-PEG-PF, SiSB-PEG, and SiSB-PF, respectively) demonstrate a

significantly smaller number of particles accumulated in cells. SiSB-PEGFA-PFFA particles showed the highest increase compared to the particles functionalized with either PFFA or PEGFA. The highest fluorescence intensity was across cells incubated with SiSB-PEGFA-PFFA particles, followed by SiSB-PFFA and then, to SiSB-PEGFA particles. This agrees with the number of folate molecules on the surface of these types of particles, see Tables 1 and S4. Thus, it is consistent with both the presence and biological activity of folate molecules on the surface of the particles.

One of the most important parameters to characterize the efficiency of specific targeting is the ratio between specific and nonspecific targeting. Comparing three differently functionalized UBMS particles with their control partners (for example, SiSB-PFFA relative to SiSB-PF), which are presented in Figure 2, one can find that the best ratios of targeted to control fluorescent signals are for SiSB-PFFA particles. These ratios are 6.7:5.4:4.6 for SiSB-PFFA : SiSB-PEG-FA : SiSB-PEGFA-PFFA particles.

Now we use the most efficient targeting particles SiSB-PFFA (and its control SiSB-PF) to verify that the mechanism of preferential targeting of folate functionalized particles does relate to folic acid receptors. To do that, we use Hs578t cells as biological control. HeLa cells overexpress folic acid receptors higher compared to MCF-7 [35-37] and MCF-10A cells. [38] Expression of folate receptors in Hs578t cells is significantly lower than that in MCF-7 cells and slightly lower than that in MCF-10 cells.[39] Hence, Hs578t cells can be used as a biological control for evaluating folic acid-mediated endocytosis of folate targeted nanoparticles. It is observed that the blue fluorescence intensity was significantly higher in HeLa cells compared to Hs578t cells when targeted with SiSB-PFFA particles, Fig.S11. Furthermore, the control SiSB-PF particles showed weak internalization with no difference between Hs578t and HeLa cells. Thus, it is plausible to say that the targeting mechanism is based on the interaction with folic acid receptors.

Toxicity study

Because our nanoparticles contain surfactant, a substance which can be harmful for cells, we investigate potential toxicity of the particles using keratinocyte cells from histologically normal human skin, see supplementary section 12 for detail. Specifically, uncoated (no PEG, no folates) nanoporous silica nanoparticles were used. The results (Table S7) show that our particles ~22 times less toxic than Triton X-100.

It is important to estimate the particle concentration for the in vivo experiments described in this work. The total blood volume of zebrafish embryos has been estimated to be 60 nL. [40] The amount of nanoparticles injected in zebrafish described in the next section is 0.5nL of 1 mg/mL concentration. Thus, the final concentration of nanoparticles in blood of the zebrafish embryo is 8.3μg/mL. This is approximately 10 times smaller than CC_{50} toxicity concentration found in cells. Note that CC_{50} was found using serum free medium. Taking into account the fact that serum substantially decreases toxic effect, toxicity of nanoparticles in zebrafish embryo blood is expected to be negligible.

Demonstration of tagging ability of UFMS particles using xenographic HeLa tumors/cells in zebrafish in vivo

Synthesized particles were further used for in-vivo testing. Zebrafish were injected in the vascularized area near the perivitelline cavity with HeLa cells. The cells were genetically altered to produce red fluorescent protein to ease identification of their location. The next day after xenografting, the cancer cells started to spread and creating metastases. 0.5 nL of 1mg/mL particles were injected behind to the eye of zebrafish. The fish was immobilized in 3% low melting agarose gel and imaged using a long working distance fluorescent microscope, see the Materials section and Supplementary information for detail.

Figure 3 shows examples of sequential imaging of metastases (red channel) and the synthesized folate functionalized fluorescent particles (blue channel). Note that hereafter the blue channel of images of zebrafish was converted into the green for better visual perception. An advantage of green color is demonstrated in Figure S18. Figure 3 A, D and G show images of tails of zebrafish (in the red channel) showing red fluorescent metastatic HeLa cells. SiSB-PEGFA, SiSB-PFFA and SiSB-PEGFA-PFFA particles images (blue channel) are shown in figure 3 B, E and H respectively. Merged channels are shown in figure 3 C, F and I.

A good co-localization of HeLa cells and folate functionalized particles is seen very well, starting from relatively large tumors (large bright spots) down to as small as ~10-20 μm. Because the small size is comparable to the size of individual HeLa cells, we may detect even individual HeLa cells. Similar images at lower resolution, in which the fish-tail is clearly seen, are shown in figure S12; regions imaged in high resolution in figure 3 are highlighted there (the areas shown in Figure 3 were chosen based on the sharpest focus and the absence of fluorescent background artifacts, which is sometimes observed presumably due to multiple reflections from the cavity of the slide used to restrain the fish). At the same time, the control non-folate fluorescent particles show noticeably less co-localization with tumors than the folate-functionalized particles (see, Figure S13 of the Supplementary information, in which one can also see the absence of how to fluorescence of HeLa cells in blue region). Also, zebrafish embryos were injected with Hs578t cells. After injecting with SiSB-PFFA particles, it was found that the particles highlighted HeLa cells and not Hs578t cells, Fig. S14. This implies that the internalization of SiSB-PFFA particles is mainly due to folic acid receptor-mediated endocytosis.

Finally, to avoid confusion of coincidental accumulation of targeting particles in particular locations of zebrafish with tumor/cancer cell targeting, a control experiment was done by injecting SiSB-PFFA nanoparticles in zebrafish, which contains no HeLa cells. Figure S17 shows the relatively smooth distribution of nanoparticles after 35 and 80 minutes. There is

no clear aggregation of nanoparticles seen. This votes in favor of the absence of coincidental targeting.

To calculate the accuracy of targeting, the obtained images were processed digitally. Calculation of sensitivity (correct identification of tumors/cancer cells) was done using multiple folate active particles, see the supplementary information for detail (Suplementray Section 11 and Table S6). As a general trend, there is an obvious increase in sensitivity with the incubation time, starting from 53% (18min) going to 90+% (80 min). At the same time, the control (no folate) particles show a rather low sensitivity of 15% even after the long incubation time (120 min). It should be noted that the purpose of these experiments is to demonstrate the in-vivo targeting ability of the ultrabright particles. Further study of sensitivity (as well as specificity) will be done in the future. In particular, it will include the optimization of particle concentration. As one can see from Table S6, 10x decrease in the particle concentration seems to be rather advantageous to improve sensitivity; it shows virtually 100% sensitivity after 100 min of incubation.

Advantage of ultrabrigthness for targeting in vivo

We now show the advantage of using ultrabrightness for the detection of metastases in zebrafish. To demonstrate it, we synthesized the same SiFB-PEGFA and SiFB-PFFA particles, but with less bright encapsulated dye, Fast Blue (FB). FB dye is not fluorescent in water but demonstrates a reasonable fluorescence after encapsulation inside of mesoporous silica particles. SiFB particles are ~100x less bright than the ultrabright ones with Stilbene dye (SiSB). The particles of both types were injected into zebrafish as described before.

Figure 4 A, C, E and G present the red HeLa metastases. Images obtained with injection of the same amount (0.5 nL of 1 mg/mL) of different fluorescent particles are shown in figures 4 B, D, F, H for less bright SiFB-PEGFA, SiFB-PFFA, and ultrabright SiSB-PEGFA, and SiSB-PFFA particles, respectively. Comparing images of the ultrabright and SiFB particles, one can see that metastases targeted with ultrabright particles show higher contrast.

To make the comparison more quantitative, we measured the contrast of multiple metastases targeted with ultrabright and less bright particles at different times. Ultrabright SiSB-PFFA particles were ~70x brighter than less bright SiFB-PFFA particles, while ultrabright SiSB-PEGFA particles were ~200x brighter than less bright SiFB-PEGFA particles. Because SiSB-PFFA and SiSB-PEGFA particles demonstrated the highest specific contrast in vitro (Figure 2), we demonstrate these measurements only for these nanoparticles. Figure 5 shows a relative contrast (the fluorescence intensity relative to the background) of tumors/cancer cells detected using SiSB-folate particles at different times after injection. One can see that at ~2 times higher contrast, which is attained ~3 times faster compared to less bright particles. It is interesting to note that longer waiting time doesn't help to reach a higher contrast when using less bright particles.

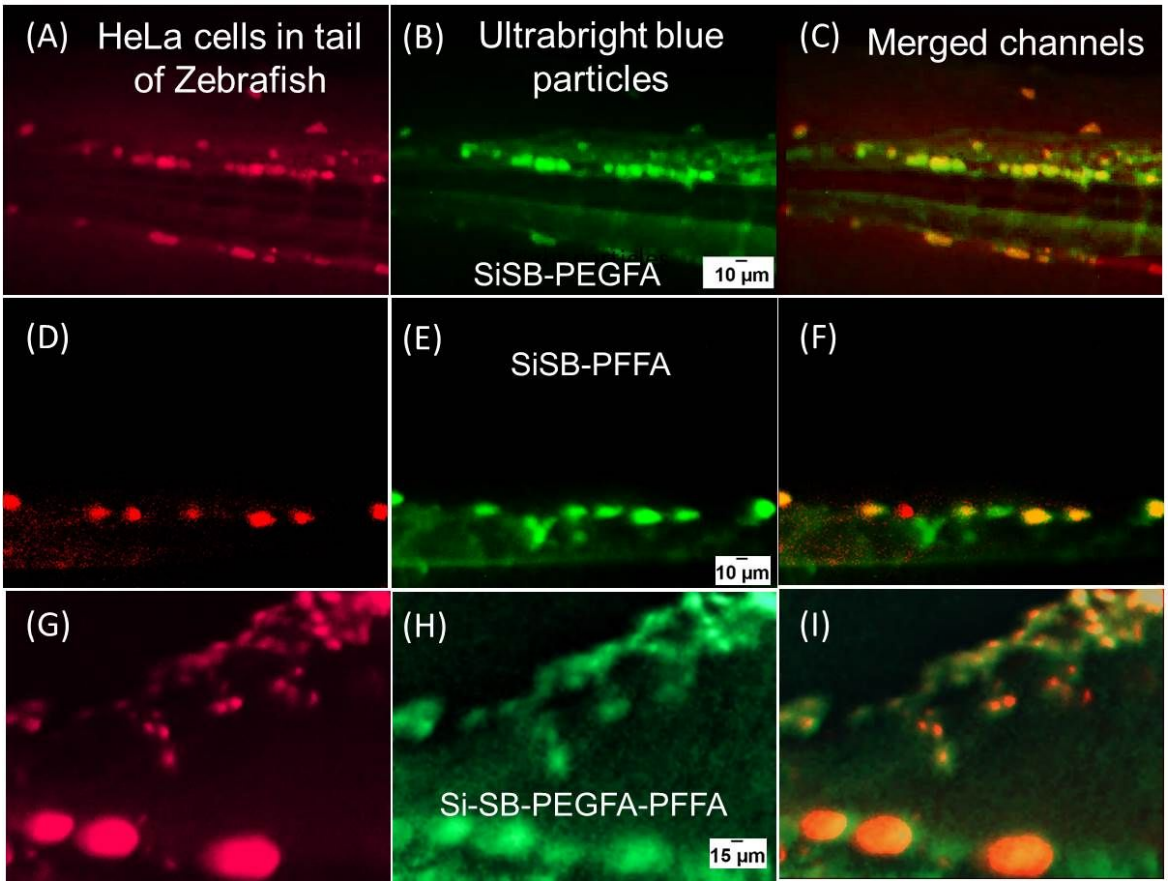

Figure 3. Co-localization of tumors and folate-functionalized UBMS nanoparticles. Zebrafish injected with red fluorescent HeLa cells in the yolk (A, D and G). Ultrabright blue fluorescent particles functionalized with PEGFA-PEG (B), PFFA (E) and PEG-FA-PFFA (H) injected close to the eye of zebrafish. Corresponding co-localization images of red fluorescent cancerous cells and particles injected in zebrafish (C, F and I). Brightness and contrast of the particles images was optimized for better viewing while keeping same values for all images. The images were taken after ~40 minutes past the particle injection.

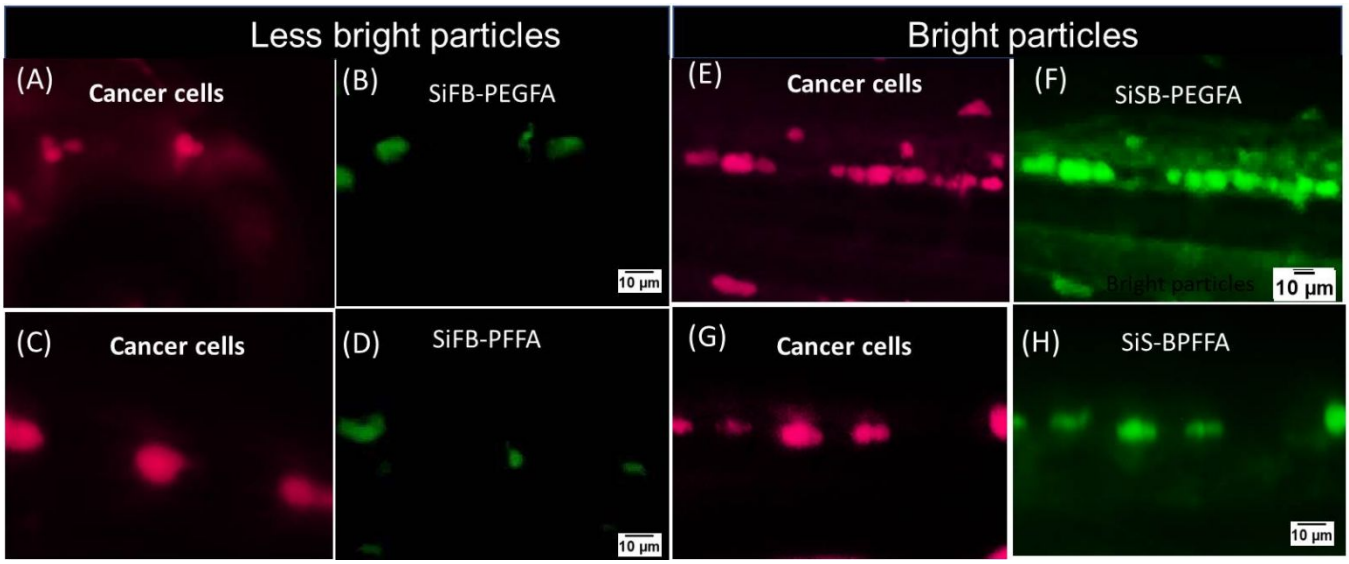

Figure 4. Zebrafish injected with red fluorescent HeLa cells in the yolk (A, E, C and G). The results are shown for less bright functionalized fluorescent particles (B) SiFB-PEGFA, (D) SiFB-PFFA and for ultrabright functionalized particles (F) SiSB-PEGFA and (H) SiSB-PFFA injected behind the eye of the zebrafish.

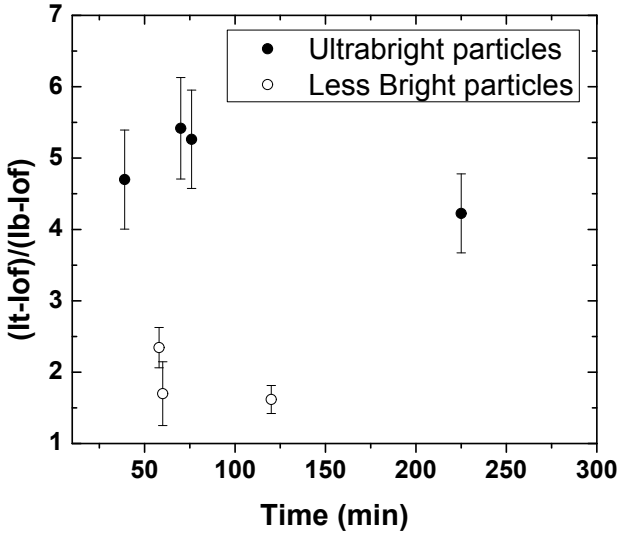

Figure 5. Relative contrasts of tumours (fluorescence of tumour relative to the background) tagged with ultrabright (SiSB- PFFA and -PEGFA) and 70-200x less bright particles (SiFB- PFFA and -PEGFA). The average relative contrast versus time since particle injection is shown. The error bar corresponds to one standard deviation.

3. Conclusion

We described the development of ultrabright fluorescent silica particles, which are suitable for in-vivo applications. We presented three ways of coating which retained ultrabrightness, covalent attachment of PEG-silane, [41] physical coating using an FDA approved copolymer PF127, and the mix of these two. In addition to PEGylation, we added folate functionality to make these particles specific to epithelial cancers (the majority of epithelial cancers overexpress folic acid receptors [42]). Folate molecules were attached to the particle surface using two methods, by using amine-modified folic acid for covalent attachment and PF127-folic acid (PFFA) conjugate for physical coating. Water-soluble and UV-fluorescent Stilbene 420 dye was used to create ultrabright fluorescent tagging silica nanoparticles. This particular spectrum was chosen to avoid interference with the fluorescence of cancer cells (in the red part of the spectrum) and the auto-fluorescence of zebrafish (green).

Besides direct PEGylation, PF127 was used to coat particles with PEG groups. It is FDA approved polymer, which therefore, is attractive for in vivo applications. Previously gold nanorods were coated with PF127 polymer by replacing CTAB on the surface of the particles. [43, 44] However, it was not reported for the coating of mesoporous silica particles, in particular in the way to preserve ultrabrightness. PF127 and PF127-folic acid conjugate [45] (PFFA) has not been reported for coating CTAB stabilized ultrabright mesoporous silica nanoparticles.

Verification of targeting activity on human cervical epithelial (HeLa) cancer cells demonstrated that the intake of the particles is proportional to the amount of folic acid attached to the particles. Addressing the challenge of targeting tumours in vivo, we measured the targeting of xenographic human cervical epithelial tumours (and presumably even

individual cancer cells) in zebrafish. We demonstrated a fast targeting on the tumours/cells. Particles were injected close to the eye and showed targeting through the entire fish body as fast as 20 min. Although coincidental colocalization of particles and HeLa cells is possible, the stability of colocalization in time and the absence of good colocalization when using Hs587t (low folate receptor) cells in favour of the specific targeting. Previous studies using zebrafish model have shown targeting after 3 hours of injection using 200 nm particles (3nL of particle suspension – no concentration was mentioned though) without any conjugation. [46]

Using our ultrabright particles, tumours (and maybe even individual cancer cells) as small as 10 microns were visualized using 1 mg/mL SiSB-PEGFA particles (figures 3 & 4). This is 37x smaller tumours than the smallest size reported previously (370 microns and sub-millimeter-sized tumours on intraperitoneal injection [47], respectively). Finally, we demonstrated the importance of ultrabrightness for fast and reliable detection of tumours/individual cancer cells. Using direct comparison with 200x less bright fluorescent particles (similar to the brightness of quantum dots), which had exactly the same surface functionalization, we demonstrated that the contrast from the targeted tumours/cancer cells was ~2 times higher and was attained ~3 times faster when using ultrabright particles. Even faster detection is quite plausible to expect. High fluorescence intensity of each particle results in less time to accumulate in the target to be detectable (become greater than background noise). Furthermore, within the time of observation (120 minutes), the less bright particles were not capable of developing the contrast comparable to the ultrabright one, even the one obtained within 18 minutes after injection. Folic acid receptors, which work as transporters, should accumulate the number of particles in time. However, the relative contrast of tumours/cancer cells (Figure 5) is not growing with time. This would presumably be explained by nonspecific targeting and possible diffusion of particles out of cells. This interesting observation will be studied in future works.

It is also worth commenting on potential leakage of dye and surfactant molecules from the particles. Although it has not been observed in physiological solutions [11] and in cells [9] even on unprotected against leakage nanoparticles, the long term behaviour of our nanoparticles in complicated in vivo environment has not been studied. We do not think it would though be a problem because nanoparticles typically do not stay long side of organisms. Secondly, even if the particles stay longer and degrade, they can release their cargo into the target organ, i.e., tumour. This would be highly useful as tumour drug delivery. Finally, the lack of leakage of surfactant is indirectly confirmed by rather low toxicity observed on cells.

4. Experimental section

Materials

Tetraethylorthosilicate (TEOS, ≥99%, GC, Sigma Aldrich), triethanolamine (TEA, reagent grade 98%, Sigma Aldrich), cetyltrimethylammonium bromide (CTAB, High Purity Grade, Amresco), (3-Aminopropyl) triethoxysilane (APTES, ≥98%, Sigma Aldrich), N-(6-aminohexyl)aminomethyl triethoxysilane (AHAMTES, 95%, Gelest), Anhydrous Dimethyl sulfoxide (DMSO, ≥99.9%, Sigma), Folic acid (FA, >97%, Sigma), Pluronic F127 (PF127, Sigma), 1,1'-Carbonyldiimidazole (CDI, Aldrich), N-hydroxysuccinimide (NHS, Sigma Aldrich), 1-ethyl-3-(3-dimethylaminopropyl)carbodiimide (EDC, Sigma Aldrich), PBS buffer, Fast Blue B salt (FB, dye content ~95%, Sigma Aldrich) and Stilbene 420 (SB, dye content ~97%, Exciton). RC membrane from Spectra/Pore of MW – 10-15kDa was used. Deionized water was used for all synthesis.

Synthesis of SB encapsulated mesoporous silica nanoparticles

Previously reported procedure was modified for synthesizing mesoporous silica nanoparticles. [11, 22] The molar ratio was 1 TEOS: 8.2 TEA: 0.23 CTAB: 142 H2O: 0.0046 SB dye. The mixture of TEOS (8.2 mmol) and TEA (67 mmol) was stirred for one minute and kept at 90˚C under quiescent conditions for 20 minutes. Another mixture of CTAB (1.9 mmol), SB dye (0.037 mmol) was stirred for 1 minute in water and kept at 60˚C for 40 minutes. The CTAB, dye and water mixture was allowed to stir at room temperature for another 15 minutes and was kept in an ice bath for 5 minutes. After 5 minutes the mixture of TEOS and TEA was then added into the aqueous solution of CTAB and dye and was stirred for further 40 minutes in an ice bath. After 40minutes the synthesis mixture was diluted with 30mL water and the excess reagents were removed by dialyzing with water using the membrane of MW 10-15kDa until no fluorescence was obtained from the dialysate (2-3 days). The pH of the mixture after dialysis was ~9. HCl was added to reduce the pH to 7.

Synthesis of PEGSilane and folic acid-amine (AHAMTES) functionalized mesoporous silica nanoparticles

PEGsilane was synthesized following the literature protocol. [41] A modified literature protocol was followed to synthesize amine-folic acid conjugate. [6] The molar ratio of TEOS:FA:PEGSilane was 1:0.0125:0.0125. The folic acid solution in DMSO (0.1mmol) was first prepared. EDC (0.51mmol) and NHS (0.41mmol) were further dissolved in the DMSO followed by stirring for 60 minutes at room temperature. AHAMTES (0.1mmol) was then added to the above solution and the mixture was stirred for another 15 minutes. The PEGSilane (PEGSilane:TEOS = 0.0125) was added into the 10-12 minutes old TEA, TEOS, CTAB, dye and water mixture followed by addition of DMSO, FA, EDC and NHS mixture. This mixture was ultrasonicated and stirred vigorously for a further 10 minutes. After 20 minutes the mixture was diluted with 30mL water and stirred for another 5 minutes. The excess reagents were removed by dialyzing with water using the membrane of MW 10-15kDa until no fluorescence was obtained from the dialysate. The pH of the mixture after dialysis was ~9. HCl was added to reduce the pH to 7.

Synthesis of PEG Silane functionalized mesoporous silica nanoparticles

Similar procedure as described in the synthesis of PEGSilane and FA-AHAMTES functionalized mesoporous silica nanoparticles was followed for synthesizing PEG Silane functionalized mesoporous silica nanoparticles except for the addition of FA and other reagents. Addition of PEG on Si-SB-PEG and Si-SB-PEG-FA: PEG (6k) was added into Si-SB-PEG and Si-SB-PEG-FA (3 mL of 1 mg/mL). Refer to supplementary information Scheme 1 for schematics of PEG silane.

Coating mesoporous silica nanoparticles with PFFA

Synthesis of PF127-folic acid (PFFA) was done following the literature protocol.[41] Refer to supplementary information Scheme 2 for schematics of PFFA. PFFA (300ul of 11mg/mL) was added and stirred stepwise (~50-100 ul per 15-30 minutes) into mesoporous silica nanoparticles (3 mL of 1 mg/mL).

Coating PEG and FA functionalized mesoporous silica nanoparticles with PFFA as done as follows. PFFA (300 ul of 11 mg/mL) was added and stirred stepwise (~50-100 ul per 15-30 minutes) into mesoporous silica nanoparticles (3 mL of 1 mg/mL).

Characterization with Dynamic light scattering (DLS)

DLS was used to measure the particle size and zeta potential of the nanoparticles. The intensity average size (Z-average) and most probable size (mean of number weighted distribution) was the average of three measurements. Typically, DLS uses the laser light of 633nm and the backscattered light is monitored over light at an angle of 173˚. 0.1ml of stock solution was diluted to 3ml deionized water before measurements. Number weighted average and Zaverage given in Table 1 are averages of three runs. Particles were weighed for determining particle concentration. Triplicates of 0.1 mL of a water suspension of particles in an aluminum foil cap were dried in a vacuum chamber for 24 hours and weighed using CAHN29 (CAHN Instruments Inc.).

Optical measurements

Cary 60 UV-Vis spectrometer from Agilent technologies was used to measure absorbance. Fluorescence was measured using the Cary Eclipse (Varian, USA), Horiba Fluorelog 3 (Horiba, Japan).

Photostability measurements were performed using Xenon lamp and Horiba Fluorolog 3 (Horiba, Japan). Dye and particles were excited using white light excitation, slit width of 14.7nm. Fluorescence was recorded every 30 seconds. Every point in figure 1D is the average of 10 data points taken every 0.1s using a slit width of 3 nm. For the rest of the study, fluorescence was measured using slit width 1 nm.

Atomic force microscopy

Icon AFM (Bruker, Inc. Santa Barbara California) with NanoScope V controller with ringing mode add-on (NanoScience solutions, Inc., Virginia) was used to image the obtained nanoparticles.

Cell cultures and fluorescent imaging

PLemR-RFP transduced, FACS sorted RFP-expressing HeLa cells and the control cells, RFP-positive Hs578t breast cancer cells that express low folic receptor levels and were acquired from ATCC, were used for the experiments. Cells were grown up to 70% confluency in DMEM medium with 10% FBS at 37C and 5% CO_2. The culture vessel was Nunc glass base dish from Thermo Fisher (Catalog number: 12-567-400). Nanoparticle stock solutions were pre-diluted directly into growth medium, mixed and added to each well for a time course. After waiting for a predefined time, the particles were washed away with PBS buffer, and cells were imaged in PBS buffer using EPI Fluorescent Inverted Microscope (TU2000 Nikon Co., Tokyo, Japan) or a Revolve Microscope (Echo, San Diego, USA). The images were taken using 10x objective (Nikon, N.A. 0.4). The high-resolution imaging was captured using oil-immersed 63x objective (Nikon, N.A. 1.4).

Establishing xenographic tumors in zebrafish and injection of nanoparticles

RFP+ human cells were harvested using Trypsin, washed 3 times, counted and resuspended in full growth medium at a final concentration of $50x10^6$ cells per mL freshly before micro-injection. All animals were handled as described in the Boston University School of Medicine zebrafish facility, in accord with our IACUC-approved protocol. Transparent *Casper* Zebrafish were bred and their embryos were raised in the dark up to 2 days post fertilization (dpf). The 2 dpf zebrafish larvae were anesthetized with Tricaine and immobilized for Hela-RFP and Hs578t-RFP cells microinjection using sharpened borosilicate glass capillaries (1.0 mm O.D. x 0,78 mm; Needles capillaries from Harvard Apparatus). The cell micro-injections were performed on WPI world precision instrument Station (Applied Scientific Instrumentation) by injection of ~1 nL of cell mixture directly into the periviteline cavity of the embryo using a micro-injection station. Zebrafish embryos were then incubated for 20 to 28 hours in the dark at 36.9ºC to allow cancer cell spreading to occur. After Hela-RFP cells widely spread (3 dpf), embryos with evident metastasis were delicately embedded in a low melting temperature agarose and micro-injected with ~0.5 nL nanoparticle solutions directly behind the eye, where the rich capillary bed is located and enables the entry of particles into circulation. Fish were imaged over time using an Olympus MVX-10 microscope (6.4x, Olympus Co., Tokyo, Japan).

Conflicts of interest

S.P. and I.S. are inventors of the ultrabright silica particles. I.S. declare interest in NanoScience Solutions, LLC (recipent of STTR NIH R41AI142890 grant). All other authors declare no conflicts of interest.

Acknowledgements

NSF CBET 1605405 and NIH R41AI142890 support are gratefully acknowledged by I.S. H.F. acknowledges grant support from NIH (CA215059), American Cancer Society (RSG-17-204-01-TBG) and the St. Baldrick's Foundation. F.J.F.L. acknowledges fellowship from Boston University Innovation Center-BUnano Cross-Disciplinary Training in Nanotechnology for Cancer (XTNC). S.A.M.A.P., S.P. and I.S. conceptualized and designed experiments related to assembly of the particles. S.A.M.A.P. did the synthesis and characterization of particles. S.A.M.A.P and S.P. discussed and did the synthesis of PF127-Folic Acid conjugate and S.A.M.A.P. did its characterization. S.P. did the synthesis of PEG-silane conjugates. S.P. acknowledges discussions with Dr. Remya P. Narayanan regarding the synthesis of folate conjugates. M.E.D. did the AFM measurements of the particle sizes. X.D.Q., F.J.F.L. and H.F. designed the in-vitro and zebrafish in-vivo experiments. X.D.Q. and F.J.F.L. conducted the in-vitro and zebrafish in-vivo experiments. S.A.M.A.P. calculated the statistics of targeting in zebrafish. I.S. and S.A.M.A.P. wrote the manuscript. All authors discussed and reviewed the manuscript.

References

1. A. B. Chinen, C. M. Guan, J. R. Ferrer, S. N. Barnaby, T. J. Merkel and C. A. Mirkin, *Chem Rev*, 2015, **115**, 10530-10574.
2. G. W. Lin, P. N. Manghnani, D. Mao, C. Teh, Y. H. Li, Z. J. Zhao, B. Liu and B. Z. Tang, *Advanced Functional Materials*, 2017, **27**, 1701418.
3. N. Melnychuk and A. S. Klymchenko, *Journal of the American Chemical Society*, 2018, **140**, 10856-10865.
4. K. Li, Z. S. Zhu, P. Q. Cai, R. R. Liu, N. Tomczak, D. Ding, J. Liu, W. Qin, Z. J. Zhao, Y. Hu, X. D. Chen, B. Z. Tang and B. Liu, *Chemistry of Materials*, 2013, **25**, 4181-4187.
5. B. Peng, M. Almeqdadi, F. Laroche, S. Palantavida, M. Dokukin, J. Roper, O. H. Yilmaz, H. Feng and I. Sokolov, *Mater Today*, 2019, **23**, 16-25.
6. S. Palantavida, N. V. Guz, C. Woodworth and I. Sokolov, *Nanomedicine: Nanotechnology, Biology and Medicine*, 2013, **9**, 1255-1262.
7. L. Wang, Q. W. Song, Q. L. Liu, D. C. He and J. Ouyang, *Advanced Functional Materials*, 2015, **25**, 7017-7027.
8. E. B. Cho, D. O. Volkov and I. Sokolov, *Small*, 2010, **6**, 2314-2319.
9. I. Sokolov and S. Naik, *Small*, 2008, **4**, 934-939.
10. V. Kalaparthi, S. Palantavida and I. Sokolov, *J. Mater. Chem. C*, 2016, **4**, 2197-2210.
11. E. B. Cho, D. O. Volkov and I. Sokolov, *Advanced Functional Materials*, 2011, **21**, 3129-3135.
12. S. Palantavida, B. Peng and I. Sokolov, *Nanoscale*, 2017, **9**, 4881-4890.
13. J. Lu, Z. Li, J. I. Zink and F. Tamanoi, *Nanomedicine: Nanotechnology, Biology and Medicine*, 2012, **8**, 212-220.
14. S. Palantavida, R. Tang, G. P. Sudlow, W. J. Akers, S. Achilefu and I. Sokolov, *Journal of Materials Chemistry B*, 2014, **2**, 3107-3114.
15. I. Sokolov and D. O. Volkov, *Journal of Materials Chemistry*, 2010, **20**, 4247–4250.
16. D. O. Volkov, E.-B. Cho and I. Sokolov, *Nanoscale*, 2011, **3**, 2036-2043.
17. J. V. Jokerst, T. Lobovkina, R. N. Zare and S. S. Gambhir, *Nanomedicine*, 2011, **6**, 715-728.
18. Y. Park, Y. M. Ryu, T. Wang, Y. Jung, S. Kim, S. Hwang, J. Park, D. J. Bae, J. Kim, H. Moon, H. S. Lim, S. Y. Kim, E. Chung, K. H. Kim, S. Kim and S. J. Myung, *Advanced Functional Materials*, 2018, **28**, 1703450.
19. Y. K. Leng, W. J. Wu, L. Li, K. Lin, K. Sun, X. Y. Chen and W. W. Li, *Advanced Functional Materials*, 2016, **26**, 7581-7589.
20. G.-F. Luo, W.-H. Chen, Y. Liu, Q. Lei, R.-X. Zhuo and X.-Z. Zhang, *Scientific reports*, 2014, **4**, 6064.
21. A. Reisch and A. S. Klymchenko, *Small*, 2016, **12**, 1968-1992.
22. J. Kecht, A. Schlossbauer and T. Bein, *Chemistry of Materials*, 2008, **20**, 7207-7214.
23. C.-S. Hsu, K.-L. Liu, K. S. Tan, H.-Y. Yen and I.-C. Chen, *The Journal of Physical Chemistry B*, 2014, **118**, 10187-10195.
24. W. C. W. Chan, D. J. Maxwell, X. H. Gao, R. E. Bailey, M. Y. Han and S. M. Nie, *Curr Opin Biotech*, 2002, **13**, 40-46.
25. W. C. W. Chan and S. M. Nie, *Science*, 1998, **281**, 2016-2018.
26. J. Lei, L. Wang and J. Zhang, *ACS Nano*, 2011, **5**, 3447-3455.
27. I. L. Medintz, H. T. Uyeda, E. R. Goldman and H. Mattoussi, *Nature Materials*, 2005, **4**, 435-446.
28. S. Santra, P. Zhang, K. Wang, R. Tapec and W. Tan, *Analytical Chemistry*, 2001, **73**, 4988-4993.
29. S. J. Lim, M. U. Zahid, P. Le, L. Ma, D. Entenberg, A. S. Harney, J. Condeelis and A. M. Smith, *Nature communications*, 2015, **6**, 8210.
30. U. Resch-Genger, M. Grabolle, S. Cavaliere-Jaricot, R. Nitschke and T. Nann, *Nature methods*, 2008, **5**, 763-775.
31. W. C. Wu, C. Y. Chen, Y. Tian, S. H. Jang, Y. Hong, Y. Liu, R. Hu, B. Z. Tang, Y. T. Lee and C. T. Chen, *Advanced functional materials*, 2010, **20**, 1413-1423.
32. E. Rampazzo, S. Bonacchi, M. Montalti, L. Prodi and N. Zaccheroni, *Journal of the American Chemical Society*, 2007, **129**, 14251-14256.
33. S. Bonacchi, D. Genovese, R. Juris, M. Montalti, L. Prodi, E. Rampazzo and N. Zaccheroni, *Angewandte Chemie International Edition*, 2011, **50**, 4056-4066.
34. C. P. Leamon and P. S. Low, *J Drug Target*, 1994, **2**, 101-112.
35. X. Zheng, K. Kelley, H. Elnakat, W. Yan, T. Dorn and M. Ratnam, *Molecular and cellular biology*, 2003, **23**, 2202-2212.
36. H. Chen, R. Ahn, J. Van den Bossche, D. H. Thompson and T. V. O'Halloran, *Molecular cancer therapeutics*, 2009, 1535-7163. MCT-1509-0045.
37. F. Sonvico, S. Mornet, S. Vasseur, C. Dubernet, D. Jaillard, J. Degrouard, J. Hoebeke, E. Duguet, P. Colombo and P. Couvreur, *Bioconjugate chemistry*, 2005, **16**, 1181-1188.
38. W. Pan, H. Yang, T. Zhang, Y. Li, N. Li and B. Tang, *Analytical chemistry*, 2013, **85**, 6930-6935.
39. R. J. Price, K. A. Lillycrop and G. C. Burdge, *Journal of nutritional science*, 2016, **5**.
40. M. P. Craig, S. D. Gilday, D. Dabiri and J. R. Hove, *Zebrafish*, 2012, **9**, 108-119.
41. V. Cauda, C. Argyo and T. Bein, *Journal of Materials Chemistry*, 2010, **20**, 8693-8699.
42. G. L. Zwicke, G. Ali Mansoori and C. J. Jeffery, *Nano reviews*, 2012, **3**, 18496.
43. D. Goh, T. Gong, U. Dinish, K. K. Maiti, C. Y. Fu, K.-T. Yong and M. Olivo, *Plasmonics*, 2012, **7**, 595-601.
44. T. Gong, D. Goh, M. Olivo and K.-T. Yong, *Beilstein journal of nanotechnology*, 2014, **5**, 546-553.
45. J.-J. Lin, J.-S. Chen, S.-J. Huang, J.-H. Ko, Y.-M. Wang, T.-L. Chen and L.-F. Wang, *Biomaterials*, 2009, **30**, 5114-5124.
46. L. Evensen, P. L. Johansen, G. Koster, K. Zhu, L. Herfindal, M. Speth, F. Fenaroli, J. Hildahl, S. Bagherifam and C. Tulotta, *Nanoscale*, 2016, **8**, 862-877.
47. A. Oseledchyk, C. Andreou, M. A. Wall and M. F. Kircher, *ACS Nano*, 2017, **11**, 1488-1497.

New ultrabright fluorescent silica nanoparticles for targeting cancers in vivo are presented.

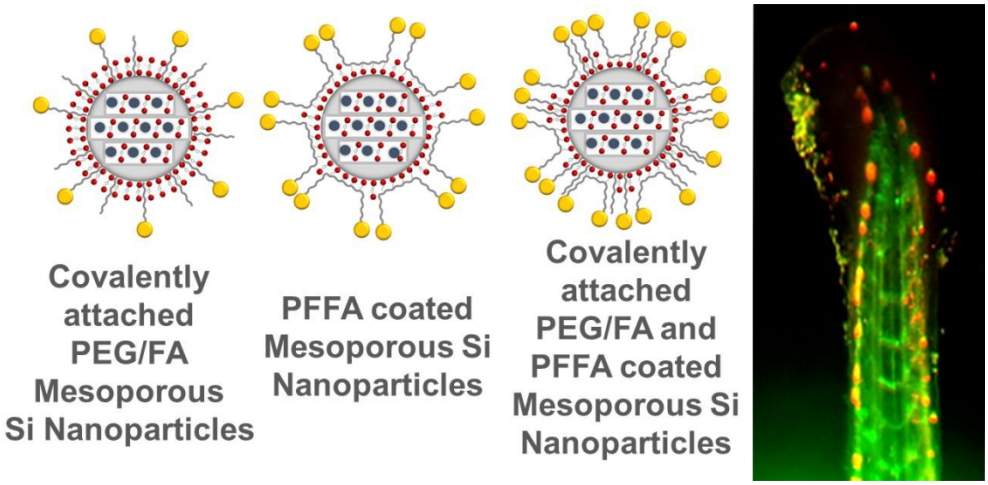

221x105mm (150 x 150 DPI)